Modelling the respiratory motion of the internal organs by using Canonical Correlation Analysis and dynamic MRI

Gang Gao[1], Jamie McClelland[1], Segolene Tarte[2], Jane Blackall[1], David Hawkes[1]

[1] *Centre for Medical Image Computing, University College London, London, WC1E 6BT*
[2] *Faculty of Classics, Oxford University, OX1 3LU*

Abstract. Radiotherapy (RT) treatments to lung tumours subject to significant respiratory motion have been proved to be difficult. By studying the respiratory motion of lung tumour from imaging modalities such as ultra-fast MRI and 4DCT, the ultimate research task is to model the tumour's respiratory motion and to use the model to predict the tumour motion. In this paper, we are proposing a method to build such a model by using a statistical technique called canonical correlation analysis. We built the model from dynamic MR volumes acquired from five volunteers. The leave-n-out (n=12) technique was used to evaluate the accuracy of the motion prediction. The motion prediction results were compared to the motion fields generated by using a B-Spline based non-rigid registration algorithm. The mean absolute differences between the two motion fields are 3.40±3.20mm, 3.62±3.08mm, 3.68±3.50mm, 4.62±3.97mm and 4.29±3.14mm. Our method is novel and efficient. Consider the model was built from low-resolution (5x5x5mm) MR volumes, the results were satisfactory. More thorough evaluations will be carried out on clinical data.

Keywords: Radiotherapy, MRI, respiratory motion model, CCA

1 Introduction

Radical radiotherapy (RT) is one of the primary treatments to non-small cell lung cancer. It uses high-energy X-Ray to kill cancer cells by causing irreparable damage to their DNA. Computed Tomography (CT), which provides high resolution anatomy and contains X-Ray attenuation need for dose calculation is usually used to plan RT procedures. However lung tumours may exhibit significant respiratory motions, limiting the accuracy of dose calculation and delivery in RT procedures. Treating lung tumours that are subject to respiratory motion has been a very active research topic in the last five years. Approaches include treating at breath hold, target delineation and dose calculations, gated treatment and tracked treatment. Except treating at breath hold, which relied on the reproducibility of the breath hold, the other three approaches require a good understanding of lung

tumour motion during respiratory cycles. However, directly tracking the tumour motion in real-time during RT treatments is difficult. The uses of implanted markers are invasive and can only measure the motions in a few locations. By studying the respiratory motion of lung tumours and its surrounding anatomy from imaging modalities like X-Ray imaging, 4DCT and MRI, it is possible to create a mathematic model which could ultimately be used to predict the tumour position [1]~[6]. Approaches to create such models have been reported in the past years. Low et al. proposed a linear model based on two continuous respiratory parameters, the volume and flow measured by spirometry [1]. The location of an internal point of interest (POI), normally in the tumour will depend on its location in the planning CT volume and the current values of the volume and air flow. A simple linear model can be built from the correlation the respiratory parameters and the positions of the POI. Khamene et al also build a model based on two respiratory parameters [2]. However the two parameters were yielded from a larger number of respiratory signals by applying Principal Component Analysis (PCA). The first two principal components (PC) were used as the respiratory parameters. In Khamene's paper, PCA was only used to reduce data dimensionality. Zhang et al extended Khamene's idea by using PCA to reduce the data dimensionality as well as to characterise the internal organ motion from the current height of the diaphragm and its height 1.5 second earlier [3]. Besides the extended application of PCA, Zhang used a free-form deformation field computed from a non-rigid registration algorithm to represent the lung tumour motions. Indeed, the non-rigid motion field does not only represent the tumour motion but also represent the motions of other internal organs, including the lungs and the diaphragm. Similar approach was used in [4][5][6]. McClelland et al found a B-Spline transformation based non-rigid registration with control points spacing of 20x20x20mm was capable of accurately representing the lung tumour motion [6]. He used a B-Spline cyclic function to model the respiratory parameters (B-Spline deformation) by using motion signals measured from a skin marker. Relatively good results were achieved.

In this paper, we propose a novel algorithm to model the respiratory motions of the internal organs and link these motions to externally monitored surrogates such as motion of the abdominal and thoracic skin surface. The algorithm involves two key steps: 1). Create the free-form deformation fields by non-rigidly registering a breath-hold reference MR volume to a set of free-breathing dynamic MR volumes; 2). Build the motion prediction model by using a statistical technique called Canonical Correlation Analysis (CCA).

In statistic, CCA is a well-known method developed by Hotelling in 1936 [7] to study the relationship between two multidimensional variables. Since its invention, CCA has been widely used in many areas including psychology, neuroscience and etc. In recent years it was used to detect neural activity in function MRI [8][9]. In this paper, we will demonstrate that CCA can also be a successful modelling technique to predict the respiratory motion. Experiments were carried out on five volunteer data sets. The results and discussion will be presented at the last sections of this paper.

2 Method

2.1 Canonical correlation analysis (CCA)

Given a p-dimensional random variable $\boldsymbol{X}$ and a q-dimensional random variable $\boldsymbol{Y}$ ($q < p$), both of which have zero mean, CCA seeks linear combinations $a\boldsymbol{X}$ and $b\boldsymbol{Y}$ such that they are maximally correlated.

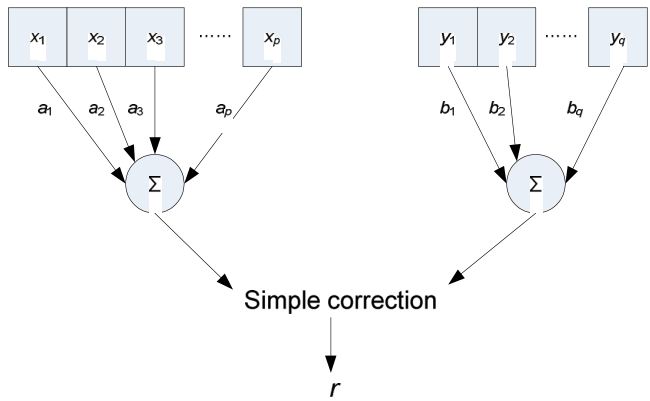

Fig.1. CCA finds the linear combination of coefficients a_1, $a_2 \ldots a_p$ and b_1, $b_2 \ldots b_q$ to gives the maximum correlation between $\boldsymbol{X}$ and $\boldsymbol{Y}$.

Fig.1 illustrates how CCA works. Canonical correlation r between $\boldsymbol{X}$ and $\boldsymbol{Y}$ can be found by solving the eigenvalue equations (equation 1).

$$\begin{aligned} C_{XX}^{-1}C_{XY}C_{YY}^{-1}C_{YX}a &= r^2 a \\ C_{YY}^{-1}C_{YX}C_{XX}^{-1}C_{XY}b &= r^2 b \end{aligned} \tag{1}$$

where C_{XY} is the covariance matrix between vectors $\boldsymbol{X}$ and $\boldsymbol{Y}$. The eigenvalue r^2 is the squared canonical correlation. a and b are the eigenvectors to the matrices $C_{XX}^{-1}C_{XY}C_{YY}^{-1}C_{YX}$ and $C_{YY}^{-1}C_{YX}C_{XX}^{-1}C_{XY}$. They are also referred to as canonical weights.
Given $\boldsymbol{U}$ and $\boldsymbol{V}$ where

$$\boldsymbol{U} = a\boldsymbol{X} \quad \boldsymbol{V} = b\boldsymbol{Y} \tag{2}$$

$\boldsymbol{U}$ and $\boldsymbol{V}$ are called canonical variates. Equation (2) is called canonical function. Up to q canonical functions can be found between p-dimensional variable $\boldsymbol{X}$ and q-dimensional variable $\boldsymbol{Y}$ ($q < p$). In principle, they must be non-correlate (orthogonal) to each other.

Canonical correlation is the maximum possible correlation between two multi-dimensional variables. The relationship between the two variables can be further investigated by analysing their canonical loadings (CL) and canonical cross loadings (CCL). By definition, CL is the covariance matrix between the original variable $\boldsymbol{X}$ or $\boldsymbol{Y}$ and its canonical variate $\boldsymbol{U}$ or $\boldsymbol{V}$. Similar to CL, CCL is the covariance matrix between $\boldsymbol{X}$

or $\boldsymbol{Y}$ and its counterpart's canonical variate $\boldsymbol{V}$ or $\boldsymbol{U}$. Equation (3) and (4) calculate CL and CCL. CL and CCL explain the amount of variable $\boldsymbol{X}$ explained by variable $\boldsymbol{Y}$ or vice versa.

$$\boldsymbol{C}_{UX} = \mathrm{Cov}(\boldsymbol{U}, \boldsymbol{X}) \quad \boldsymbol{C}_{VY} = \mathrm{Cov}(\boldsymbol{V}, \boldsymbol{Y}) \tag{3}$$

$$\boldsymbol{C}_{VX} = Cov(\boldsymbol{V}, \boldsymbol{X}) \quad \boldsymbol{C}_{UY} = Cov(\boldsymbol{U}, \boldsymbol{Y}) \tag{4}$$

Equation (4) is equivalent to matrix equation (5)

$$\boldsymbol{V} = \boldsymbol{C}_{VX}\boldsymbol{X} \tag{5}$$

From equation (5) we have

$$\boldsymbol{X} = \boldsymbol{C}_{VX}^{-1}\boldsymbol{V} \tag{6}$$

By combining equation (6) and equation (2), we have

$$\boldsymbol{X} = \boldsymbol{C}_{VX}^{-1}\mathrm{b}\boldsymbol{Y} \tag{7}$$

Equation (7) is considered as a prediction model which characterises vector $\boldsymbol{X}$ by using vector $\boldsymbol{Y}$. Considering vector $\boldsymbol{X}$ as the internal organ motion signals and vector $\boldsymbol{Y}$ as the surrogate signals measured from the skin surface, equation (7) estimates the internal organ motion from the surrogate signals. By using equation (7), we presume that the correlation between the internal motion and the external motion does not change over time. A higher CL or CCL means more elements in $\boldsymbol{X}$ or $\boldsymbol{Y}$ contribute to the construction of the model, suggesting the possibility of a more accurate prediction. This theory will be proved by our experimental results.

2.2 Relationship between CCA and PCA

CCA and PCA are similar to each other in two ways. Firstly, both CCA and PCA are linear subspace methods. Secondly, both of them solve the same equation (equation 8).

$$\mathbf{B}^{-1}\mathbf{A}\boldsymbol{w} = r^2\boldsymbol{w} \tag{8}$$

In fact equation (8) is equivalent to equation (1) given

$$\mathbf{A} = \begin{bmatrix} 0 & C_{XY} \\ C_{YX} & 0 \end{bmatrix}, \mathbf{B} = \begin{bmatrix} C_{XX} & 0 \\ 0 & C_{YY} \end{bmatrix} \text{ and } \boldsymbol{w} = \begin{pmatrix} a \\ b \end{pmatrix}$$

However, PCA are fundamentally different with CCA because it solves equation (8) by using different matrices $\mathbf{A}$ and $\mathbf{B}$. In PCA, matrix $\mathbf{A}$ equals to C_{XX}, matrix $\mathbf{B}$ is a constant $\boldsymbol{I}$.

2.3 Internal organ motion

Dynamic MR volumes had high temporal resolution (0.5s for a full 3D volume) and a large field of view (480x480x265mm) showing the skin surface and the internal organs, but had a low spatial resolution (5x5x5mm). A breath-hold high resolution MR volume (1.875x1.875x2mm) was acquired when the subject was instructed to hold the breath. Dynamic MR volumes were non-rigidly registered to the reference volume using a B-Spline registration algorithm [11]. The B-Spline control point grid contained 2250 control points (15x15x10 with 40x40x40mm spacing), each of which had a 3D displacement (*dx, dy, dz*). The displacement vector ***D*** for the registration result is given by:

$$\boldsymbol{D} = [dx_1, dy_1, dz_1, \ldots, dx_n, dy_n, dz_n]$$

Here, $n = 2250$.

Applying CCA directly to the displacement vector ***D*** is computationally prohibited. PCA, a dimensionality reduction technique was performed to reduce the number of the internal organ motion variables to *n* principal components (PC). Zhang et al chose the first two PCs which covered more than 83% of variance to build their model [3]. However, for the datasets we used, we need three PCs to represent around 80% of the variations.

Given the control point motion ***D***, the PCs ***P***. Equation (9) estimates the original variables.

$$D` = \overline{D} + \sum_{k=1}^{K} \lambda_k P_k \approx D \tag{9}$$

where λ is the principal component coefficient.

2.3 Skin motion

The skin surface is clearly visible in the dynamic MR volumes, and its position can be measured automatically using a threshold algorithm similar to the method used in [4] (fig.2). 6 control points were manually picked from the thoracic and the abdominal areas. For each control point, current position m_t and its precursor position m_{t-2} were measured to form the skin motion signals.

$$\boldsymbol{M} = [m_{1,t1}, m_{1,t2}, \ldots\ldots m_{6,t1}, m_{6,t2}]$$

where

$$m_{i,t2} = \begin{pmatrix} m_{i,t-2}(t \geq 2) \\ m_{i,t+j-2}(t \leq 2) \end{pmatrix}$$

By adding a precursor position $m_{i,t-2}$ we had the advantage that it incorporated temporal correlations into the model, distinguishing the inspiration and expiration portions of the breathing cycle.

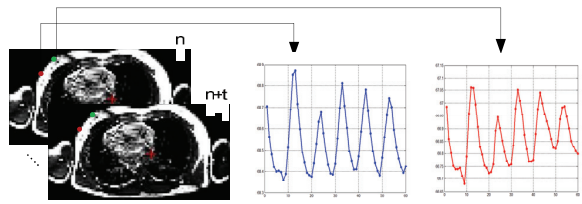

Fig.2. Skin motions were measured from the dynamic MR volumes by using a threshold based segmentation algorithm.

The input variables to CCA must be zero mean. Equation (10) calculates the standarised motion signals.

$$M^* = \frac{(M - \overline{M})}{std(M)} \tag{10}$$

Given the PCs of the internal organ motions $\boldsymbol{P}$, and the skin motions $\boldsymbol{M}$, CCA calculates CCL $\boldsymbol{C}$ and canonical weight b between $\boldsymbol{P}$ and $\boldsymbol{M}$**.** From equation (7) we have

$$\boldsymbol{P} = \boldsymbol{C}^{-1} b \boldsymbol{M}^* \tag{11}$$

By using equation (9) and (11), the estimated control point displacements $\boldsymbol{D'}$ can be calculated from the real-time measurement of the skin motion.

3 Experiment results

3.1 Spectrum of PCA Eigenvalues

For all the volunteers, PCA was applied to the internal control point displacements to reduce the number of variables from 6750 to 3 PCs. For the five volunteers, the first three eigenvalues account for 86.3%, 82.0%, 76.5%, 95.9% and 85.4% of the total variance in the data.

3.2 CCA

The CCA function was implemented in Matlab (The MathWorks, USA) statistics toolbox. The two parameters of CCA were the PCs of the internal motions and the skin motions. For all the five volunteer datasets, the skin motion variables had strong canonical correlations with the internal motion variables. The mean correlations between the three

pairs of canonical variables were 0.983 ± 0.007, 0.825 ± 0.08 and 0.595 ± 0.07. CL and CCL measured the strength of overall relationships between the skin motions and the internal organ motions. The mean cumulative sums of CL for the five datasets were 0.83, 0.89, 0.87, 0.65 and 0.80 respectively. The mean cumulative sums of CCL or the five datasets were 0.70, 0.83, 0.83, 0.54 and 0.77. The higher the cumulative sum of CL or CCL is, the more likely the model can deliver a satisfactory result. In the fourth dataset, we observed considerably lower values of CL and CCL. This indicated the motion predicted by the model built from the fourth dataset might not be as accurate as the models built from the other datasets.

3.3 Model evaluation

Five separate CCA models were built from the volunteer MR data. The registration results were assessed visually by an expert. Four out of five dataset were considered to be registered successfully. For one dataset, the registration results exhibit more than two voxel misalignment in the borders of the chest and the lungs. The leave-n-out strategy was adopted to evaluate the performance of the CCA models. From each of the datasets, 12 volumes which cover at least one respiratory cycle were dropped. The models were built from the other 48 volumes and used to predict the deformation fields of the missing volumes. Fig.3 shows the deformation field at an arbitrarily selected point inside the dynamic volume and the predicted deformation field at this point from one of the five CCA models. Generally the organ respiratory motions in the anterior-posterior direction (Y) and the left-right direction (Y) are not as considerable as the motion in the foot-head (Z) direction. Therefore the motion signals in x and y directions were easier to be contaminated by noise. Fig.3a and fig.3b show our attempt to model and predict the noisy signals. Fig.3c shows the predicted deformation field is closely matched the measured deformation field in Z direction. We calculated the mean absolute difference (MAD) between the predicted deformation fields and the deformation fields generated by a B-Spline-based non-rigid registration algorithm. For the five datasets, the MADs are 3.40 ± 3.20mm, 3.62 ± 3.08mm, 3.68 ± 3.50mm, 4.62 ± 3.97mm and 4.29 ± 3.14mm. Fig.4 shows the MAD maps generated from the B-Spline control points around the lungs in the mid-coronal slices (Y=0). It is clear that most of the errors are around 5mm. In some extreme cases, the differences can be up to 12mm because of the noise, the image registration errors and the surrogate signal measurement errors. The motion prediction errors around the lungs in the 4^{th} volunteers are bigger than the errors in other subjects because of two major reasons. 1). The volunteer has a fast respiratory rate and the temporal resolution of the dynamic MRI (0.5s/volume) is insufficient to produce an accurate motion prediction model; 2). Considerable errors were produced by the image registrations.

The cumulative sums of CL and CCL of the fourth dataset are considerably lower than those of the other four datasets. The experimental data prove the theory that the signal

prediction from the CCA model with high cumulative sum of CL or CCL is not as accurate as the prediction from the model with high cumulative sum of CL or CCL.

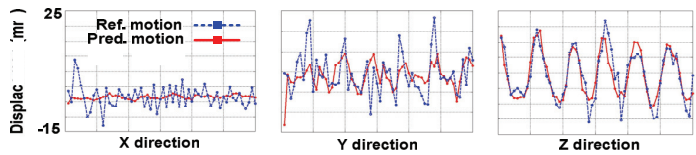

(a) (b) (c)

Fig.3. 12 volumes were dropped successively from the dynamic MR volumes. A leave-n-out strategy was used to predict the motion signals measured from the missing 12 volumes. From an arbitrarily selected point inside the MR volume, the predicted motion signals are closely matched the measured motions in Z direction. In X, Y and Z directions, the mean errors are 2.86 ± 2.40mm, 3.62 ± 3.16mm and 2.89 ± 2.37mm.

Generally, the results are satisfactory considering our models were built from low-resolution MRI with 5x5x5mm voxel spacing. Therefore, the errors correspond to about one voxel.

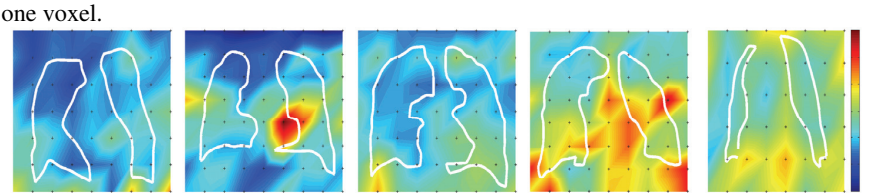

Fig.4 The MAD maps were calculated from the mid-coronal slices (Y=0) showing that most of the prediction errors around the lungs are approximately 5mm. The motion prediction errors around the lungs in the 4th subject were higher because of the large image registration errors. The white contours outline the boundary of the lungs and the dark spots suggest the locations of the B-Spline control points.

4 Discussion and conclusions

We proposed an algorithm to model the respiratory motion of the internal organs by using CCA and MRI. In this pilot study, CCA models were built from dynamic MR volumes acquired from five volunteers. By using the leave-n-out strategy, the deformation fields of the dynamic MR volumes were successfully predicted by using our model (average error is less than 1 voxel). Although we only used the skin motions to build and drive the model, it did not mean the skin surface was the only surrogate source possible with our

model. Without any modification, the model could be adapted to more parameters due to the nature of the CCA method.

Similar to Khamene's method, our model was built from 3D dynamic MR volumes while many other reported methods involved the uses of cine mode CT [1][3][6]. CT volumes acquired in cine mode often contain discontinuities in the data between adjacent couch position due to sorting errors and inter-cycle variation. Extra procedures are needed to correct the artifacts caused by these discontinuities [3]. By using an ultra-fast MR sequence, it is possible to acquire the whole 3D anatomy of the lung from one scan. Furthermore, by using MRI, it is possible to conduct a relatively long scan. 30 seconds MR data were acquired from each of the datasets in this study. Compared to other studies (24 seconds in [2], 20 seconds in [6], 11 seconds in [1] and one respiratory cycle in [3]), our data cover more respiratory cycles sampling more inter-cycle variation. Potentially, more data can be acquired with MR if required. But for CT studies, it is difficult to increase the data acquisition time due to the radiation dose limit.

Many of the methods mentioned in the introduction use polynomial or cyclic function to model the respiratory cycles. By using these methods, a presumption was made that the end positions of inspiration and expiration remained the same over time. However, this presumption is obviously wrong as the end respiratory positions can vary more than 10mm (fig.3) in reality. Our method did not make such presumption. It modeled the whole respiratory signals including the inter-cycle variation. In this study, our models were built from 48 dynamic MR volumes and used to predict the internal organ motions shown in the other 12 MR volumes. Reasonable results were achieved. Without the radiation dose limit, we can acquire more MR volumes and potentially can build a even more accurate model. Zhang et al. reported a method to build the respiratory motion model by using PCA [3]. Similar to CCA model, PCA model can also model the inter-cycle variation of the respiratory motion. But the use of CT has efficiently limited the acquisition time. In fact, Zhang's CT data only covered one respiratory cycle.

Although our approach has many unique advantages and the uses of MRI to plan RT procedures are beneficial (see Introduction), we have not yet evaluated our model on clinical data. Therefore, the clinical accuracy of our model remains unknown. Having an efficient and successful respiratory motion model is a big step toward. But it is still a significant challenge to put this model into clinical use. Other known issues such as tumour baseline variation and morphology changes [11] should be accounted for in any clinical system and we are exploring how our model may be quickly and accurately updated using interfraction imaging (kV or MV fluoroscopy or cone-beam CT).

References

1. Low, D. A, Nystrom, M, Kalinin E, et al., "A method for the reconstruction of four-dimensional synchronized CT scans acquired during free breathing," Med. Phys. 30, 1254-1263 (2003).

2. Khamene, A, Warzelhan, J K, Vogt ,S, et al., "Characterization of internal organ motion using skin marker positions," MICCAI 2004, 526-533 (2004).
3. Zhang, Q H., Pevsner, A, Hertanto, A, et al., "A patient-specific respiratory model of anatomical motion for radiation treatment planning", Med. Phys. 34, 4772 (2007).
4. Blackall, J M, Ahmad, S, Miquel, M E, et al., "MRI Based Measurement of Respiratory Motion Variability and Assessment of Imaging Strategies for Radiotherapy Planning," *Phys. Med. Biol.* 51, 4147-4169 (2006).
5. Zeng, R, Fessler, J A, and Balter, J M, "Estimating 3-D respiratory motion from orbiting views by tomographic image registration," *IEEE Trans. Med. Imaging* 26, 153-163 (2007).
6. McClelland, J R, Chandler, A G, Blackall, J M, et al., "A Continuous 4D Motion Model from Multiple Respiratory Cycles for Use in Lung Radiotherapy", Med. Phy., 33, 3348-3358 (2006)
7. Hotelling, H., "Relations between two sets of variates", Biometrika, 28, 321–377 (1936)
8. Worsley, K., J., Poline, J-B, Friston, K., J., Evans, A., C., "Characterizing the response of PET and fMRI data using multivariate linear models", Neuroimage, 6, 305–319 (1997).
9. Friman, O., Carlsson, J., Lundberg, P., et al., "Detection of neural activity in functional MRI using canonical correlation analsyis", Magnetic Resonance Medicine, 45, 323-330 (2001).
10. Rueckert, D, Sonoda, L I, Hayes, C, et al., "Nonrigid registration using free-form deformations: application to breast MR images," *IEEE Trans. Med. Imaging* 18, 712–721 (1999).
11. Sonke, J J, Lebesque, J, and van Herk, M, "Variability of four-dimensional computed tomography patient models," *Int. J. Radiat. Oncol., Biol., Phys.* 70, 590-598 (2008).